JOURNAL OF VETERINARY MEDICAL RESEARCH 2019, 26 (2): 258-270

Journal homepage:
http://www.bsu.edu.eg/bsujournals/JVMR.aspx

Online ISSN: 2357-0520 Print ISSN: 2357-0512

Original Research Article

Cross-sectional anatomy, magnetic resonance imaging and computed tomography of fetlock joint in camel

Ibrahim, A.A.H.*, **Adam, Z.E. and Tawfiek, M.G.**
Anatomy and Embryology Department, Faculty of Veterinary Medicine, Beni-Suef University, Beni-Suef 62511, Egypt.

ABSTRACT

The current study aimed to describe the normal cross sectional anatomy, magnetic resonance imaging and computed tomography of fetlock joint in adult camel from both sexes. The study was carried out on twelve fetlock joints of fresh cadavers from three camels. The case history of these camels indicated that they were grossly normal with no orthopedic disorders. The cadaveric fetlock joints (n=12) were scanned using CT scanner and a 1 Tesla MRI scanner, injected with colored latex and sectioned into transverse, dorsal and sagittal slices. Cross anatomical sections were correlated with their corresponding CT and MR images for evaluation of the normal relevant anatomical structures which appeared with different signal intensities on CT and MRI scans. The current study revealed that all major soft tissues in fetlock joint of camel were clearly visualized on both CT and MR images, except the short and cruciate sesamoidean ligaments which could not be identified on both CT and MR images. The anatomical sections with the corresponding CT and MR images obtained in this study could be used as a reference for diagnosis and interpretation of clinical diseases in fetlock joint of camel.

ARTICLE INFO

Article history:
Received 29/4/ 2019
Accepted 30/7/2019
Online 2/8/2019

Keywords:
Camel, Computed tomography, Fetlock joint, Magnetic resonance imaging.

***Corresponding author: Ibrahim, A.A.H.**, Anatomy and Embryology Department, Faculty of Veterinary Medicine, Beni-Suef University, Beni-Suef 62511, Egypt.
Email: d.azzamohamed88@gmail.com

1. Introduction

Camel is adapted to hard climate of the desert and has the capability to survive and produce under hard environmental conditions (Sadegh et al., 2007). Concurrently, it is used as an important source of milk, meat and hide especially in developing countries (Ahmad et al., 2010). Moreover, camel is considered as an essential source in sport and tourism in the Gulf region (Farah and Fischer, 2004).

Lameness is a serious worldwide problem due to its negative economic impact on dairy farms (Solano et al., 2015). Moreover, lameness in camel has a different pattern when compared to bovine and equine, because of peculiar anatomy and biomechanics of camel (Al-Juboori, 2013). These instances require awareness of the normal anatomical structure and developing of modern diagnostic imaging techniques for identification and evaluation of orthopedic problems. Recently, there is a growing awareness for using computed tomography (CT) and magnetic resonance imaging (MRI) as valuable diagnostic imaging modalities in veterinary practices (Bienert and Stadler, 2006; Nuss et al., 2011). However, their limited accessibility, high costs and the need for animal general anesthesia diminish the use of these techniques in veterinary practices (Arencibia et al., 2000). Nevertheless, improvement in availability and accessibility of these tools increases the demand for their use in animals (Pollard and Puchalski, 2011). These techniques are not only used for diagnostic purposes, but also can be used in several biometric researches and measurements (Onar et al., 2002).

Even though many CT and MRI studies had been done on animal digits (Badawy, 2011; El-Shafey and Abd Al-Galil, 2012; El-Shafey and Kassab, 2012; El-Nahas et al., 2015 in camel, Raji et al., 2008; Raji et al., 2009; Al-Akraa et al., 2014 in bovine, Sampson et al., 2005; Sampson and Tucker, 2007 in horse). More details on cross sectional anatomy of the fetlock joint of dromedary camel in correspondence to CT and MRI are still needed.

The present study aimed to provide a comprehensive detailed anatomic reference on the cross sectional anatomy, CT and MRI of the fetlock joint in camel to be used as a helpful database for interpretation and evaluation of musculo-skeletal disorders in fetlock joint of these animal species.

2. Materials and methods

2.1. Animals

CT and MRI examination were performed on twelve fetlock joints (right and left) of fresh cadavers from three dromedary camels (2-4 years old, weighed about 350-500 kg.). These cadaveric limbs (fore and hind limbs) were obtained from a local slaughter-house at Beni-Suef Governorate, the camels of these specimens were grossly normal with no fetlock joint disorders. This examination was done within four hours after euthanasia. Then the limbs were frozen and sectioned for preparation of transverse, dorsal and sagittal slices 1cm thickness.

2.2. Magnetic resonance imaging

Limbs (n=12) were positioned with their palmar/plantar aspect as the dependent portion and their long axis perpendicular to the examination table. T1-weighted MR images (TR=1900ms, TE=2.74ms, slice thickness= 2mm) were acquired in transverse, sagittal and dorsal planes using a 1 Tesla magnet (Philip Medical System Intera).

2.3. Computed tomography

Limbs (n=12) were placed on the examination table as MRI study. Toshiba Alexion CT scanner was used for obtaining bone and soft tissue windows CT scans in transverse, dorsal and sagittal planes. The acquisition settings were 120 KV and 250 MA with 2mm slice thickness.

2.4. Preparation of the anatomical cross sections

The scanned specimens (n=12) were injected with colored gum-milk latex. The needle was introduced into the dorsal pouches of the fetlock joint abaxial to the tendinous portion of the digital extensor tendons. The limbs were frozen at -20°C for one week, and then sectioned into transverse (Forelimb; n=2, hind limb; n=2), dorsal (Forelimb; n=2, hind limb; n=2) and sagittal (Forelimb; n=2, hind limb; n=2) slices starting about 10cm dorsal to the fetlock joint till the middle of the first phalanx in 1cm slice thickness using an electric band saw. All anatomic sections were gently cleaned using tap water and then photographed. The anatomical sections were inspected, identified and selected in correlation to their correspond-ding CT and MR images.

2.5. Comparison of cross anatomical sections with CT and MR images

The cross anatomical sections of the fetlock joint were compared to their correspond-ing CT and MR images on the basis of shape and location and tissue density properties. For evaluation of the most clinically relevant anatomical structures of the fetlock joint in camel of the same specimens, six CT and MR images were selected to be representative for the anatomical structures (Fig. 1) in their matched anatomical sections, one in a sagittal plane (Fig. 2), two in dorsal planes (Figs. 3, 4) and three in transverse planes (Figs. 5-7).

3. Results

The obtained anatomical cross sections were selected and compared with their corresponding CT and MR images in a sagittal plane (Fig. 2), dorsal planes (Figs. 3, 4) and transverse planes (Figs. 5-7). No significant morphological or topographical variations were observed between fetlock joints of the fore and hind limbs, or between the right and left contralateral limbs.

3.1. Magnetic resonance imaging (MRI)

Articular cartilages were clearly recogni-zed from the surrounding bony structures as a thin layer of high signal intensity (Figs. 2, 4). Subchondral bone appeared as a thin plate of low signal intensity and could be easily differentiated from articular cartilage at the proximal extremity of each bone (Figs. 2, 4). Cancellous bone could be visualized at the extremities of each bone with heterogeneous high signal intensity (Figs. 2, 4). Cortical bone had low signal intensity, while the medulla had high signal intensity (Figs. 2, 4). However, the trabecular pattern of bones could not be differentiated on obtained MR images. Proximal sesamoid bones were best recognized on transverse MR images (Fig. 6).

Soft tissue structures were clearly visualized in all MR images with variable signal intensities. Extensor tendons could be recognized on MR images included; lateral and common digital extensor tendons, these tendons had homogenous low signal intensity. Margins of these tendons were well-defined by the surrounded fascia which appeared as low intermediate signal intensity. Extensor tendons were best evaluated on transverse MR images as three narrow strips on dorsal aspect of the distal end of metacarpus/ metatarsus (Figs. 5-6). At the level of the proximal phalanges, the extensors appeared as four structures indicated division of the lateral limb of common digital extensor tendon into two branches which could be visualized as small oval structures on the dorso-medial aspect of each digit (Fig. 7).

On palmar/plantar aspect of distal end of metacarpus/metatarsus, the inter-osseous muscle (suspensory ligament) could be clearly visualized as an elongated structure with a low signal intensity deep to digital flexor tendons at a level about 4cm proximal to the fetlock joint, this muscle appeared as four oval structures representing the axial and abaxial proximal sesamoidean ligaments on transverse MR images (Fig. 5). However, inter- osseous muscle and its branches were best evaluated on dorsal MR

images at the level of sesamoid bones (Fig. 2). Moreover, branches of the inter-osseous muscle could be depicted on sagittal MR images (Fig. 2).

Digital flexor tendons appeared with a homogenous low signal intensity structures surrounded by digital tendon sheath which had low signal intensity. On the transverse MR images, SDFT appeared as an incomplete ring around oval-shaped DDFT until the level of the proximal extremity of the first phalanx (Figs. 5-7). On dorsal MR images, SDFT appeared as two branches on both sides of DDFT, and then it changed its position to be deep to DDFT (Fig. 3). This reposition of the flexor tendons could be also recognized on sagittal MR images (Fig. 2). Moreover, manica flexoria had a high signal intensity which best recognized on transverse (Fig. 5) and dorsal (Fig. 3) MR images.

Joint capsules of fetlock appeared with low signal intensities, margins of these capsules were clearly outlined as a thin line of intermediate signal intensity on sagittal (Fig. 2), dorsal (Fig. 4) and transverse (Figs. 6, 7) MR images. However, ligaments of this joint were well-defined and clearly outlined on transverse and dorsal MR images with heterogeneous intermediate signal intensity (Figs. 3-7), while straight sesamoidean ligament and annular ligament could be identified on sagittal MR images (Fig. 2). Ligaments of the fetlock joint which could be clearly identified on MR images included; suspensory, collateral, collateral sesamoi-dean, palmar/plantar and straight sesamoidean ligaments. While short and cruciate sesamoidean ligaments could not be defined.

3.2. Computed tomography

The bone window provided an excellent delineation between the cortical and subcortical tissues as well as bone medulla with a clear differentiation of trabecular patterns. This medulla appeared hypo dense black in color. Diaphysis, condyles, sagittal ridges, proximal sesamoid bones and phalanges appeared hyper dense with smooth margins on transverse, dorsal and sagittal CT images (Figs. 2-7).

In soft tissue window, bones appeared as hyperdense structures, while the soft tissues were depicted with variable densities. On dorsal aspect of the fetlock joint, extensor tendons; lateral digital extensor as well as medial and lateral limbs of common digital extensor were visualized as hyperdense structures compared with the surrounded hypodense connective tissues. These tendons were best recognized on transverse CT images as three narrow strips on dorsal aspect of the metacarpus/metatarsus (Fig. 5). At the level the proximal phalanges, these extensors appeared as four structures indicating the division of lateral limb of common digital extensor tendon into two branches which appeared as small oval structures on dorso-medial aspect of limb (Figs. 6, 7).

On palmar/plantar aspect of distal end of metacarpus/metatarsus, the inter-osseous muscle (suspensory ligament) could be clearly visualized at a level about 4cm proximal to the fetlock joint as four oval structures representing the axial and abaxial proximal sesamoidean ligaments on transverse CT images (Fig. 5). However, the inter-osseous muscle and its branches were best evaluated on dorsal CT images at the level of sesamoid bones (Fig. 3). Moreover, branches of the inter-osseous muscle could be depicted on sagittal CT images (Fig. 2).

Digital flexor tendons could be recognized as hyperdense structures surrounded by hypodense connective tissues on palmar/ plantar aspects of the fetlock joint on transverse, dorsal and sagittal CT images. On transverse CT images, SDFT appeared as an incomplete ring around oval-shaped DDFT until the level of proximal extremity of the first phalanx (Figs. 5-7).

On dorsal CT images, SDFT appeared as two branches on both sides of DDFT, and then it changed its position to be deep to DDFT (Fig. 3). This reposition of the flexor tendons could be also recognized on sagittal CT images Manica flexoria appeared as a well-defined (Fig. 2). hypodense structure on transverse (Fig. 5) and dorsal (Fig. 3) CT images.

Joint capsule of the fetlock joint appeared as a hypodense structure on sagittal (Fig. 2), dorsal (Fig. 4) and transverse (Figs. 5-7) CT images. However, ligaments of this joint were well-defined on transverse and dorsal CT images as hyperdense structures with surrounding hypodense connective tissues (Figs. 4-7). While straight sesamoidean and annular ligaments could be identified on sagittal CT images (Fig. 2). On CT images the ligaments of fetlock joint could be clearly identified included; suspensory, collateral, collateral sesamoidean, palmar/plantar and straight sesamoidean ligaments. While short and cruciate sesamoidean ligaments could not be recognized.

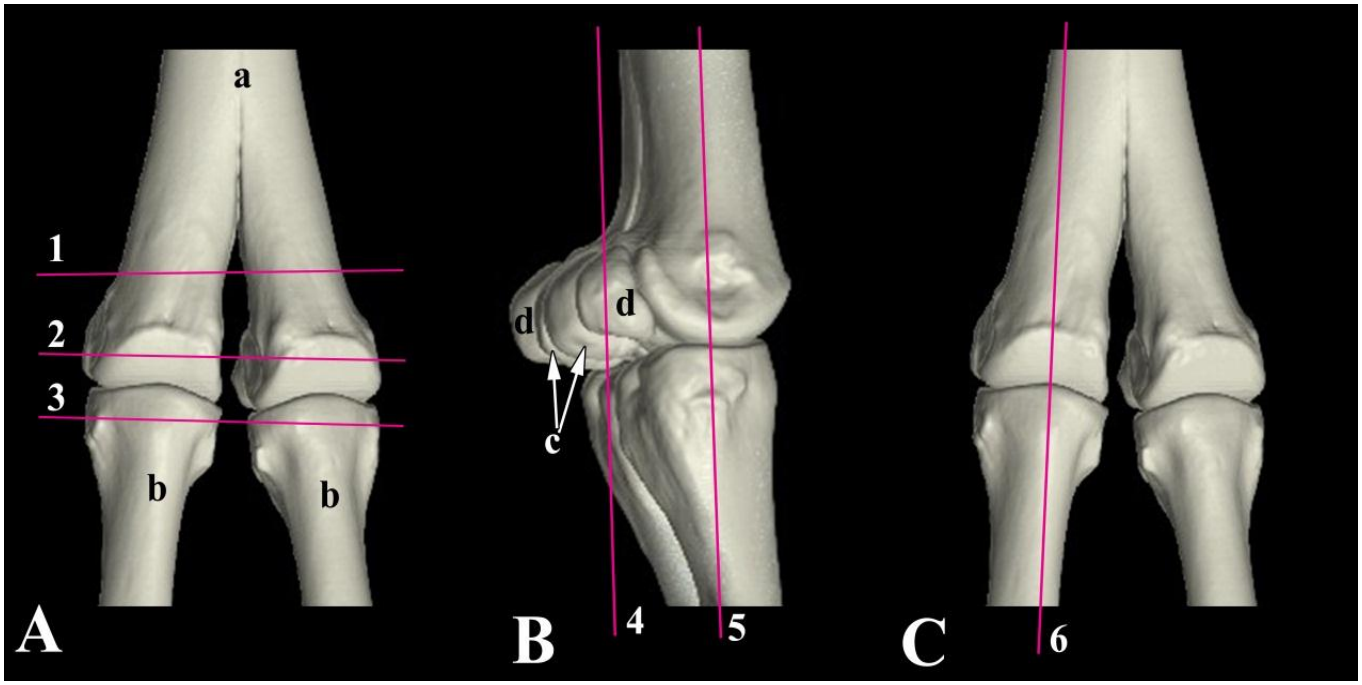

Fig. 1 Three dimensional reconstructed computed tomographic views of fetlock joint of camel. Numbered planes indicated the approximate levels of cross anatomical sections and their corresponding magnetic resonance imaging and computed tomographic depictions: A- Dorsal view showing the selected planes for transverse sections (1-3); B- Lateral view showing the selected planes for dorsal sections (4, 5); C- Dorsal view showing the selected planes of sagittal sections (6); a- Metacarpus/ metatarsus; b- First phalanx; c- Axial sesamoid bones; d- Abaxial sesamoid bones.

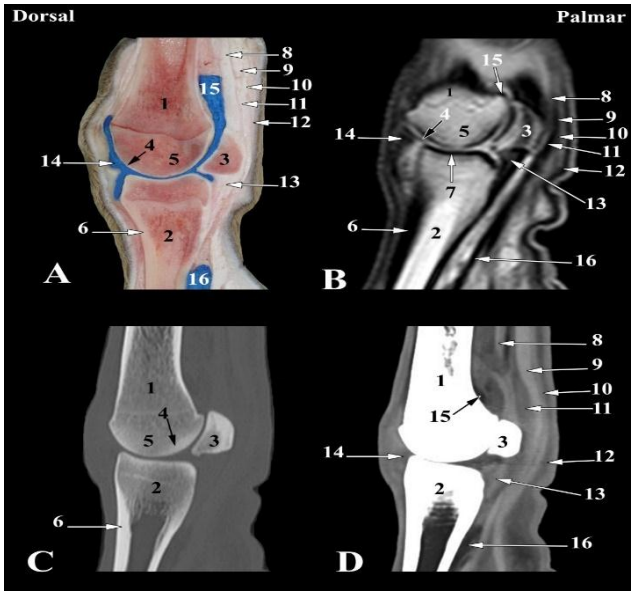

Fig. 2 Sagittal images of right fore fetlock joint of camel (level 6 as indicated in Fig. 1). A- Sagittal anatomical section; B- Magnetic resonance image; C- Bone window computed tomography image; D- Soft tissue window computed tomography image: 1- Metacarpus; 2- First phalanx; 3- Proximal sesamoid bone; 4- Articular cartilage; 5- Cancellous bone; 6- Cortical bone; 7- Subchondral bone; 8- Suspensory ligament; 9- Deep digital flexor tendon; 10- superficial digital flexor tendon; 11- Manicaflexoria; 12- Annular ligament; 13- Straight sesamoidean ligament; 14- Dorsal synovial pouch of fetlock joint; 15- Palmar synovial pouch of fetlock joint; 16- Palmar synovial pouch of pastern joint.

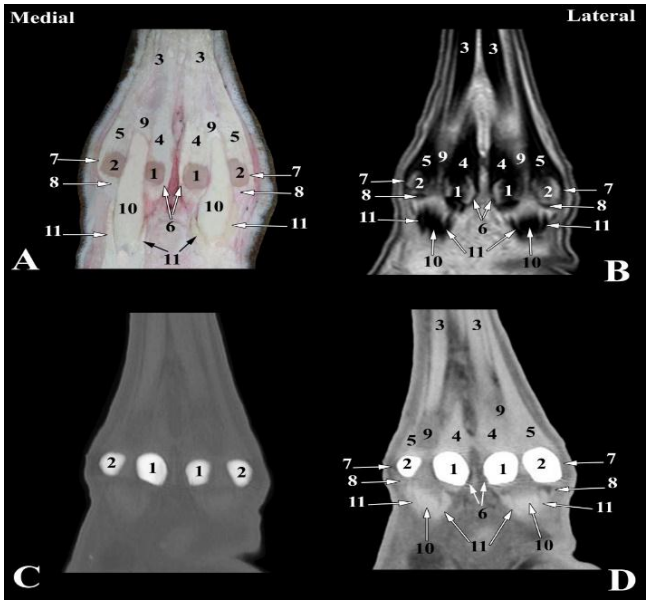

Fig. 3 Dorsal images of right hind fetlock joint of camel at the level of proximal sesamoid bones (Level ٤ as indicated in Fig. 1). A- Dorsal anatomical section; B- Magnetic resonance image; C- Bone window computed tomography image; D- Soft tissue window computed tomography image: 1- Axial sesamoid bones; 2- Abaxial sesamoid bones; 3- Inter-osseous muscle; 4- Axial limbs of inter-osseous muscle; 5- Abaxial limbs of inter-osseous muscle; 6- Axial collateral sesamoidean ligaments; 7- Abaxial collateral sesamoidean ligaments; 8- Straight sesamoidean ligaments; 9- Manica flexoria; 10- Deep digital flexor tendon; 11- Superficial digital flexor tendon.

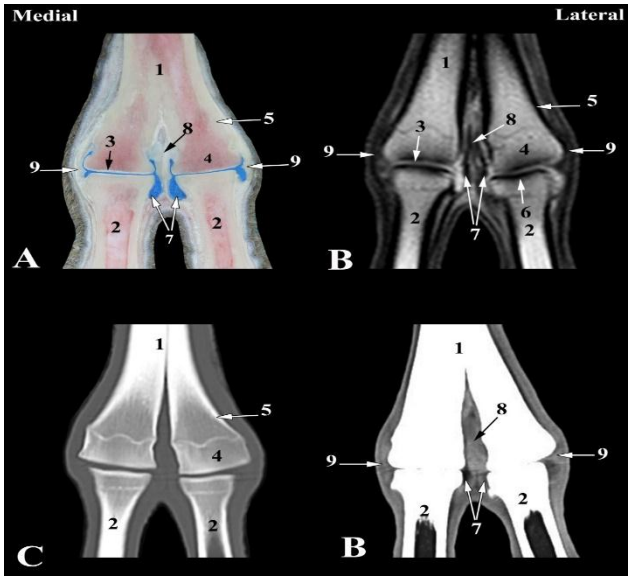

Fig. 4 Dorsal images of fetlock joint of camel at the level of collateral ligaments attachment (Level 5 as indicated in Fig. 1). A- Dorsal anatomical section; B- Magnetic resonance image; C- Bone window computed tomography image; D- Soft tissue window computed tomography image: 1- Metacarpus; 2- Proximal phalanx; 3- Articular cartilage; 4- Cancellous bone; 5- Cortical bone; 6- Subchondral bone; 7- Joint cavity of fetlock joint; 8- Axial collateral ligaments of fetlock joint; 9- Abaxial collateral ligaments of fetlock joint.

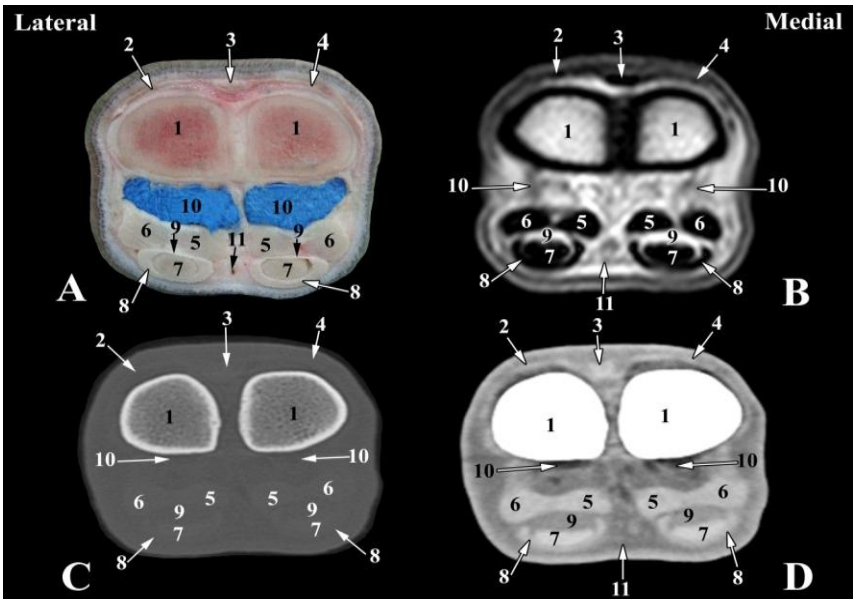

Fig. 5 Transverse images of right fore fetlock joint of camel at the level of metacarpal/metatarsal trochlea (Level 1 as indicated in Fig. 1). A- Transverse anatomical section; B- Magnetic resonance image; C- Bone window computed tomography image; D- Soft tissue window computed tomography image:1- Metacarpus; 2- Lateral digital extensor tendon; 3- Lateral limb of common digital tendon; 4- Medial limb of common digital extensor tendon; 5- Axial limbs of inter-osseous muscle; 6- Abaxial limbs of inter-osseous muscle; 7- Deep digital flexor tendon; 8- Superficial digital flexor tendon; 9- Manica flexoria; 10- Palmar synovial pouch of fetlock joint; 11- Common palmar digital artery.

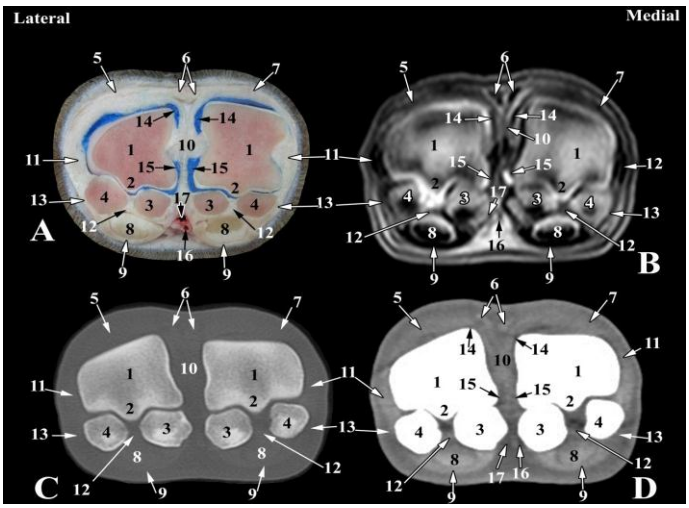

Fig. 6 Transverse images of right fore fetlock joint of camel at the level of middle of proximal sesamoid bones (Level 2 as indicated in Fig. 1). A- Transverse anatomical section; B- Magnetic resonance image; C- Bone window computed tomography image; D- Soft tissue window computed tomography image:1- Metacarpus; 2- Palmar sagittal ridge; 3- Axial sesamoid bones; 4- Abaxial sesamoid bones; 5- Lateral digital extensor tendon; 6- Lateral limb of common digital extensor tendon; 7- Medial limb of common digital extensor tendon; 8- Deep digital flexor tendon; 9- Superficial digital flexor tendon; 10- Axial collateral ligaments of fetlock joint; 11- Abaxial collateral ligaments of fetlock joint; 12- Palmar ligament of fetlock joint; 13- Collateral sesamoidean ligaments; 14- Dorsal synovial pouch of fetlock joint; 15- Palmar synovial pouch of fetlock joint; 16- Common palmar digital artery; 17- Common palmar digital vein.

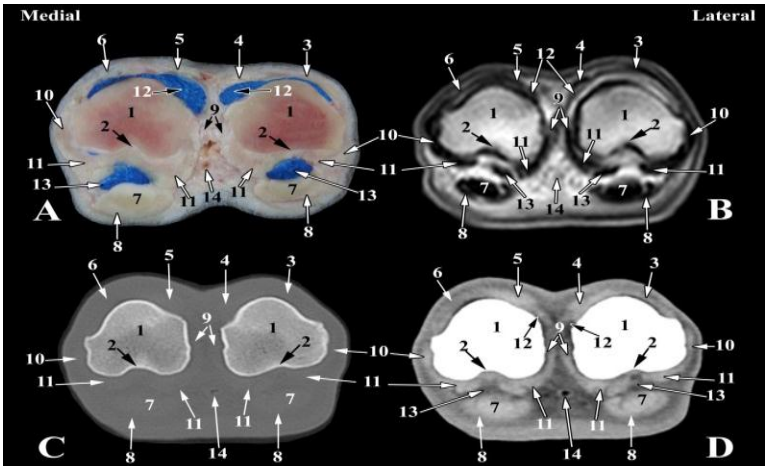

Fig. 7 Transverse images of left hind fetlock joint of camel at the level of proximal phalanges (Level 3 as indicated in Fig. 1). A- Transverse anatomical section; B- Magnetic resonance image; C- Bone window computed tomography image; D- Soft tissue window computed tomography image: 1- Proximal phalanx; 2- Trochlear fovea of proximal phalanx; 3- Lateral digital extensor tendon; 4- Lateral branch of lateral limb of common digital
extensor tendon; 5- Medial branch of lateral limb of common digital extensor tendon; 6- Medial limb of common digital extensor tendon; 7- Deep digital flexor tendon; 8- Superficial digital flexor tendon; 9- Axial collateral ligaments; 10- Abaxial collateral ligaments; 11- Straight sesamoidean ligaments; 12- Dorsal synovial pouch of fetlock joint; 13- plantar synovial pouch of fetlock joint; 14- Common plantar digital artery.

4. Discussion

The compared anatomical cross sections with their corresponding CT and MR images provided detailed views for the most normal relevant structures of the fetlock joint in camel. These images could be used as a normal anatomic reference during diagnosis of the musculoskeletal disorders in this region.

CT and MRI were excellent imaging modalities used for scanning of fetlock joint in camel. These modalities permitted visualization of the clinically relevant structures in three planes and serial slices allowing evaluation of these structures at several angles. Moreover, using latex injected joint cavities allowed a precise description of anatomical features of this joint, and gave a standard clinical reference for the position and shape of the normal anatomical structures. CT images were acquired with minimal slice thickness and interstice space providing an accurate spatial resolution and decrease partial volume artifacts, as well as a T1-weighted MRI sequence was adjusted with minimal slice thickness at a high acquisition speed; these acquisitions allowed more detailed anatomical structures to be feasible for practical clinical imaging (Smith et al., 2011).

Due to the peculiar anatomy of the distal limb in camel and high risk of lameness which may affect the draft ability (Al-Juboori, 2013), using a high definitive diagnostic technique is very important. However, radiography is the main technique for evaluation of musculo-skeletal disorders due to its entire differentiation of the bony structures, ready accessibility and low cost (Kinns and Nelson, 2010), this technique causes superimposition and over-lapping of the soft tissues (Van Der Vekens et al., 2011). Ultrasonography is non-invasive technique cannot penetrate the bones and cartilages (Samii et al., 1998), so it gives a small field of view and each structure has to be depicted separately, and a cross-sectional study through the entire digit is difficult (Denoix et al., 1993). Nevertheless, ultrasonography is used well for visualization of separate ligaments and tendons (Lisher and Walliser, 2005). Therefore, CT and MRI are excellent diagnostic techniques providing a better evaluation of soft tissues (Raji et al., 2008; Seddek et al., 2014; Abedallaah et al., 2015; Hagag and Tawfiek, 2018). Moreover, these modalities give good spectrum views of the cross sectional imaging helping in diagnosis of the abnormalities and the extent of the lesions (Raji et al., 2009).

Although, CT permits high detailed osseous structures and can distinguish bony changes before they are radiographically or clinically apparent (Young et al., 2007), and can be used for evaluation of soft tissue structures (Raji et al., 2008; Seddek et al., 2014). However, MRI can simultaneously permit imaging of bone and soft tissue with a higher soft tissue contrast than CT, and no risk of ionizing radiation, in matching the findings of and Hagag and Tawfiek (2018). In agreement with El-Nahas et al. (2015) in camel and Hagag and Tawfiek (2018) in cattle CT bone window allowed differentiation between cortex and medulla. Moreover, the present study showed that CT bone window images provided more delineated trabecular pattern than MR images. The bony elements of the distal end of the metacarpus/ metatarsus, proximal end of first phalanx and sesamoid bones were outlined in this study using CT as hyperdense with smooth margins. Similar results were observed in cattle (Raji et al., 2008), camel (Badawy, 2011), buffalo and camel (El-Shafey and Kassab, 2012), cattle and buffalo (Al-Akraa et al., 2014) and cattle (Hagag and Tawfiek, 2018). Moreover, the medulla of these bones appeared hypodense and black in color, similarly with the results of Raji et al. (2008) in cattle and Badawy (2011) in camel.

Using MRI in this study, articular cartilages, cortical bone, subchondral bone, cancellous bone were clearly outlined and well-evaluated. Articular cartilages were evaluated on MRI not on CT images, where they recognized from the surrounding bony structures as a thin layer of high signal intensity. Similar

findings were reported by Hagag and Tawfiek (2018) in cattle. On the other hand, the articular cartilage could be observed using CT in horse (Vanderperren et al., 2008). Cohen et al. (1999) attributed this difficult imaging to markedly curve articular surfaces of the distal limb and too thin cartilages for the spatial resolution in clinical MRI. Using MRI in this study, Subchondral bone appeared as a thin plate of low signal intensity and could be easily differentiated from articular cartilage at proximal extremity of each bone. Cancellous bone could be visualized at extremity of first phalanx with heterogeneous high signal intensity. Cortical bone had low signal intensity. Similar findings were observed by Hagag and Tawfiek (2018) in cattle. The present study showed that medulla of distal end of the metacarpus/metatarsus and proximal end of first phalanx had high signal intensity on MRI and it appeared hypodense and black in color on CT images. On contrary to that it appeared with low signal intensity in cattle (Raji et al., 2009) and camel (El-Shafey and AbdAl-Galil, 2012), while it as dark shade in CT images (Raji et al., 2008 in cattle and Badawy, 2011 in camel**)**.

The current study revealed that all major soft tissues in distal limb of camel were clearly visualized on both CT and MR images. However, it was difficult to identify the cruciate and short sesamoidean ligaments on CT and MR images, in agreement with El-Shafey and Kassab (2012), El-Shafey and Sayed-Ahmed (2012) and El-Shafey and Abd Al-Galil (2012) in camel and Hagag and Tawfiek (2018) in cattle. However, the two ligaments were only identified using CT images including; collateral ligaments and collateral sesamoidean ligaments (El-Nahas et al., 2015 in camel). While, all ligaments of the fetlock joint in horse could be outlined and recognized on CT images except the collateral sesamoidean and short distal sesamoidean ligaments (Vanderperren et al., 2008).

The present study and Hagag and Tawfiek (2018) in cattle observed that the ligaments of the fetlock joint were visualized with heterogeneous intermediate signal intensity using MR images. While, these ligaments were well-defined on CT images as hyper dense structures with surrounding hypodense connective tissues, similarly to the findings of El-Nahas et al. (2015) in camel.

The extensor and flexor tendons were clearly outlined in cross anatomical sections and their corresponding MR and CT images in the current study. However, these tendons could be demonstrated in the cross anatomical sections only after dissection of the intervening fascia (El-Shafey and Abdel Al-Galil, 2012 in camel and El-Shafey and Sayed-Ahmed, 2012 in camel and buffalo**)**.

In agreement with Hagag and Tawfiek (2018) in cattle these tendons appeared as hyperdense with surrounding hypodense connective tissue on CT images, while they are visualized on MR images as homogenous low signal intensity. Moreover, the deep digital flexor tendon was depicted on CT images by El-Nahas et al. (2015) in camel as a hyperdense structure. In addition to that on MR images, the SDFT appeared rounded with low signal intensity, and the DDFT appeared oval in shape, low intensity and clear outlines (El-Shafey and Abd Al-Galil, 2012 in camel**)**. Moreover, the present study and Hagag and Tawfiek (2018) in cattle depicted the digital sheath as a thin layer of low signal intensity on MR images. Moreover, this sheath was visualized on CT images as a hypodense connective tissue surrounding digital flexor tendons, in a similar to the results of Puchalski et al. (2007) in horse.
In addition to that, the current study permitted a detailed visualization of the manica flexoria in cross anatomical sections, CT and MR images. Moreover, this structure was depicted, in this study, with a high signal intensity which best recognized on transverse and dorsal MR images, while it appeared as a well-defined hypodense structure on transverse and dorsal CT images. This manica flexoria is clearly visible in CT images surrounding the deep digital flexor

tendon proximal to the fetlock joint of horse (Vanderperren et al., 2008). On the other hand, it is demonstrated only in cross sectional anatomy of buffalo, while in camel it could not be visualized either in cross anatomical sections or on CT images (El-Shafey and Kassab, 2012 and El-Shafey and Sayed-Ahmed, 2012).

The inter-osseous muscle was clearly recognized in this study in cross anatomical sections, CT and MR images, where it appeared as a hyperdense structure on CT images and it had low signal intensity on MR images. Moreover, this muscle appeared an elongated structure deep to digital flexor tendons, while, at the level about 4cm proximal to the fetlock joint, this muscle appeared as four oval structures representing the axial and abaxial proximal sesamoidean ligaments. While Al-Akraa et al. (2014) reported that the inter-osseous muscle appears on the palmar aspect of the metacarpal bone in both CT images and cross sections as an elongated or flattened structure in cattle and elliptical in buffalo. However, El-Shafey and Sayed-Ahmed (2012) in buffalo and camel observed this muscle more distinctly in cross sections than in CT images.

The joint capsule of fetlock appeared in this study with low signal intensity, margins of this capsule were clearly outlined as a thin line of intermediate signal intensity on transverse, dorsal and sagittal MR images. Similar findings were observed in fetlock joint of cattle (Hagag and Tawfiek, 2018). Moreover, this capsule appeared as a hypodense structure on transverse, dorsal and sagittal CT images, similar to the findings of El-Nahas et al. (2015) in camel. On contrary, this joint capsule cannot be observed using CT or MR images, due to they are potential cavities appear only in linear cross sections (El-Shafey and Abd Al-Galil, 2012in camel; El-Shafey and Kassab, 2012 in camel and buffalo;Al-Akraa, et al., 2014 in cattle and buffalo**)**.

5. Conclusion

The current study provided definite anatomical cross sections with their corresponding CT and MR images of the most clinically relevant structures of fetlock joint in camel. These images could be used as a normal anatomic reference during diagnosis of the musculoskeletal disorders in this region.

References

Abedallaah B, Awaad AS, Elhawari SF, Sharshar AM (2015). Normal brain of one-humped camel: a study with magnetic resonance imaging and gross dissection anatomy. Indian Journal of Veterinary Surgery, 36(1): 46-50.

Ahmad S, Yaqoop M, Hashmi M, Ahmad S, Zaman MA, Tariq M (2010). The economic importance of camel: A unique alternative under crisis. Park Vet. J., 30(4): 191-197.

Al-AKraa AM, El-Kasapy AH, El-Shafey AA (2014). Intra-articular injection, computed tomography and cross sectional anatomy of the metacarpus and digits of the cattle (*Bostaurus*) and buffalo (*Bosbubalis*). Global Veterinaria, 13(6): 1122-1128.

Al-Juboori A (2013). Prevalence and etiology of lameness in racing camels (*Camelus dromedarius*) in Abu Dhabi Emirate. Journal of Camelid Science, 6: 116–121.

Arencibia A, Vazquez JM, Rivero M, Latorre R, Sandoval JA, Vilar JM, Ramirez JA (2000). Computed tomography of normal craniocephalic structures in two horses. Anat. Histol. Embryol., 29: 295–299.

Badawy AM (2011). Computed tomographic anatomy of the forefoot in one-humped camel (*Camelus dromedaries*). Global Veterinaria, 6(4): 417-423.

Bienert A, Stadler P (2006): Computed tomographic examination of the locomotor apparatus of horses a review. Pferdeheilk, 22: 218-26.

Cohen ZA, McCarthy DM, Kwak SD, Legrand P, Fogarasi F, Ciaccio EJ Ateshian GA (1999). Knee cartilage topography, thickness,

and contrast areas from MRI: In-vitro calibration and in vivo measurements. Osteoarthritis and Cartilage, 7: 95-109.

Denoix JM, Crevier N, Roger B. Lebas JF (1993). Magnetic resonance imaging of the equine foot. Veterinary Radiology and Ultrasound, 6: 405-411.

El-Nahas A, Hagag U, Brehm W, Ramadan RO, Al Mubarak A, Gerlach K (2015). Computed tomography of the hind limbs in healthy dromedary camel foot. U. of K. J. Vet. Med. Anim. Prod., 6(2): 98-102.

El-Shafey AA, Abd Al-Galil ASA (2012). Magnetic resonance image of the one-humped (*Camelusdromedarius*) digits. Journal of American Science, 8(9): 549-556.

El-Shafey AA, Kassab A (2012). Computed tomography and cross sectional anatomy of the metatarsus and digits of the one-humped camel (*Camelus dromedaries*) and Egyptian water buffalo (*Bosbubalis*). Anat., Histol., Embryol., 42: 130-137.

El-Shafey AA, Sayed-Ahmed A (2012). Computed tomography and cross sectional anatomy of the metacarpus and digits of the one-humped camel and Egyptian water buffalo. Journal of American Science. 8(9): 549-556.

Farah Z, Fischer A (2004). Milk and meat from the camel: Handbook on products and processing publishing. Zurich, Switzerland: ETH Univ. Publishing. Hochschuleverlang AG ander ETH Zurich, pp15-28.

Hagag U, Tawfiek MG (2018). Ultrasonography, computed tomography and magnetic resonance imaging of the bovine metacarpo/metatarso-phalangeal joint. The veterinary Journal, 233: 66-75.

Kinns J, Nilson N (2010). Imaging tarsal trauma. Equine Veterinary Education, 22(6): 296-298.

Lisher CJ, Kishimoto U (2005). Fracture of the paracondylar process in four horses: advantages of CT imaging. Equine Veterinary Journal, 37(5): 483-487.

Nuss K, Schnetzler C, Hagen R, Schwarz A, Kircher P (2011). Clinical application of computed tomography in cattle. Tierarztl PraxAusg G Grosstiere Nutztiere, 39: 317-324.

Onar V, Kahvecioglu KO, Cebi V (2002). Computed tomography analysis of the cranial cavity and neurocranium in the German shepherd dog (Alsatian) puppies. Veterinary Archive, 72: 57-66.

Pollard R, Puchalski S (2011). CT contrast media and applications. In: Veterinary computed tomography. Schward, T. and Saunders J. (eds), Willey-Blackwell, pp 57-65.

Puchalski SM, Galuppo LD, Hornof WJ, Wisner ER (2007). Intra-arterial contrast-enhanced computed tomography of the equine distal extremity. Veterinary Radiology and Ultrasound, 48(1): 21-29.

Raji AR, Sardari K, Mohammadi HR (2008). Normal cross-sectional anatomy of the bovine digit: comparison of computed tomography and limb anatomy. Anat., Histol., Embryol., 37: 188-191.

Raji AR, Sardari K, Mohammadi HR (2009). Magnetic resonance imaging of the normal bovine digit. Veterinary Research Communication, 33: 515-520.

Sadegh BAM, Shadkhast S, Sharifi A, Mohammadnia HR (2007). Lacrimal apparatus system in one-humped camel of Iran *(Camelus dromedarius):* Anatomical and radiological study. Iranian Journal of Veterinary Surgery, 2(5): 76-80.

Samii VF, Briller DS, Koblic PD (1998). Normal cross-sectional anatomy of the feline thorax and abdomen: comparison of computer tomography and cadaver anatomy. Veterinary Radiology and Ultrasound, 39: 504-511.

Sampson SN, Schmeider RK, Tucker RL (2005). Magnetic resonance imaging of the equine distal limb.in: equine surgery. 3rd ed. Auer JA, Stick JA (eds) Philadelphia: Saunders, pp 946-963.

Sampson SL, Tucker RL (2007). Magnetic resonance imaging of the proximal metacarpal and metatarsal regions. Clinical Technical Equine Practice, 6: 78-85.

Seddek AM, Abedellaah BA, Awaad AS (2014). Computed tomography and dissection anatomy of the frontal and maxillary sinuses in native Egyptian goats. Indian Journal of Veterinary Surgery, 35(1): 12-16.

Smith MA, Dyson SJ, Murray RC (2011). The appearance of the equine metacarpo-phalangeal region on high-field vs standing low-field magnetic resonance imaging. Vet. Radiology and Ultrasound, 52: 61-70.

Solano L, Barkema HW, Pajor EA, Mason S, LeBlanc SJ, Zaffino-Heyerhoff JC, Nash CG, Haley DB, Vasseur E, Pellerin D (2015). Prevalence of lameness and associated risk factors in Canadian Holstein-Friesian cows housed in free stall barns. Journal of Dairy Science, 98: 6978–6991.

Vanderperren K, Ghaye B, Hoegaerts M, Saunders JH (2008). Evaluation of Computed Tomographic Anatomy of the Equine metacarpophalangeal Joint. American Journal of Veterinary Research, 69: 631-638.

Vand Der Vekens E, Gergman EH, Van Der veen H, Vanderperren K, Raes EV, Puchalski SM, Bree HJ, Saunders JH (2011). Computed tomographic anatomy of the equine stifle joint. American Journal of Veterinary Research, 72: 512-521.

Young BD, Samii VF, Mattoon JS, Weibrode SE, Bertone AL (2007). Subchondral bone density and cartilage degeneration patterns in osteoarthritic metacarpal condyles of horses. American Journal of Veterinary Research, 68: 841-849.